Defect and Diffusion Forum
ISSN: 1662-9507, Vol. 434, pp 173-182
doi:10.4028/p-ls2bVE

Submitted: 2023-09-29
Accepted: 2024-05-20
Online: 2024-08-22

Charge Carrier Capture by Prominent Defect Centers in 4H-SiC

Orazio Samperi[1,a*], Lasse Vines[2,b], Anders Hallén[3,c] and Maria Elena Fragalà[1,d]

[1]Department of Chemical Sciences, University of Catania, 95125 Catania, Italy

[2]Centre for Material Science and Nanotechnologies, University of Oslo, 0373 Oslo, Norway

[3]KTH Royal Institute of Technology, SE 164 40 Kista, Sweden

[a]orazio.samperi@phd.unict.it, [b]lasse.vines@fys.uio.no, [c]ahallen@kth.se, [d]me.fragala@unict.it

Keywords: 4H-SiC, junction DLTS, capture cross-section, capture energy barrier, entropy factor.

Abstract. The knowledge of capture properties of electrically active defects is of primary importance as it helps to understand which deep states are effective in controlling the excess free carriers' lifetime. Combining DLTS capture experiments with thermal emission measurements enables an overall thermodynamic description of deep states, thus making it possible to characterize recombination centers in semiconductor-based devices. In the present study, junction DLTS capture rate measurements were employed to extract the true capture cross-sections (inversely proportional to the carrier lifetime) and capture energy barriers for the main lifetime limiting defects in 4H-SiC (silicon carbide). A peculiar forward bias dependence of the capture parameters was observed for the *shallow* boron (B) hole trap. Capture rate measurements on the *deep* boron (D-center) trap also evidenced the presence of two capture mechanisms, thus allowing discrimination of D_1 and D_2 deep states within the D-center DLTS peak. The results were combined with activation energies and apparent capture cross-sections to obtain the free energy (ΔG) of electronic activation for the analysed deep states.

Introduction

Advances in recent years in the growth of 4H-SiC epitaxial layers have led to industrial scaling of SiC based device manufacturing for the power electronics market. 4H-SiC based power devices are a matter of fact, but a stimulating discussion on this material is still running both in the context of material engineering and at the theoretical level as well, with a particular interest in the so-called defect engineering. A thorough knowledge of point defects influencing the electrical and/or optical properties and the understanding of the mechanisms underlying their behaviour are required for material engineering and Technology Computer-Aided Design (TCAD) device modelling.

Many of the electrically and optically active defects in 4H-SiC have been identified by combining Deep Level Transient Spectroscopy (DLTS), Photoluminescence (PL), and Electron Paramagnetic Resonance (EPR) measurements. Further, the literature is quite rich of experimental data and *ab initio* calculations on 4H-SiC defects thermodynamics. In particular, the $Z_{1/2}$ trap state – originating from the (0/2-) double acceptor transition of carbon vacancy V_c [1] – has been recognized as one of the main lifetime killers in n-type 4H-SiC [2], and attention has been put on localized charge carrier lifetime control by intentional defect creation/annihilation. The presence of high cross-section boron-related defects in n-type 4H-SiC - due to boron contamination during the epitaxial growth - has been also detected, and a deep species (named *deep* boron, or D-center) has been recognized as a potential trap for holes, limiting the performance of bipolar devices or n-type detectors [3]. Indeed, the importance of boron on the charge carrier lifetime was recently revisited by Ghezellou, where it was shown that B can limit minority carrier lifetime in high quality epitaxial layers [4].

DLTS has played a major role in measuring thermodynamic and kinetic quantities - including defect formation enthalpy, capture cross-section, capture energy barrier, entropy factor and, consequently, the free energy of electronic activation of the defect - but, while activation energies and apparent capture cross-sections are well known quantities, there are still open questions in the literature about entropy factors and capture energy barriers for several of the electrically active defects

in 4H-SiC. Such data are required to achieve a complete picture of the defect thermodynamics and to help understanding the recombination centers behaviour.

Information on the free carrier capture of deep states is provided by capture rate measurements. The experiment can be performed both for majority and minority carrier traps, using junction DLTS. With the correct approximations, the true capture cross-sections and capture energy barriers can be extracted by taking advantage of the temperature dependence of the capture process. Combining these quantities with the trap signature obtained from classic DLTS thermal emission measurements makes it possible to estimate the free energy (ΔG) of electronic activation for the given defect. From the practical point of view, the capture experiment is straightforward for capture of majority carriers by majority carrier traps, while extraction of the same quantities for capture of minority carriers by minority carrier traps is more cumbersome.

The work we describe here can be placed within this family of experiments. We present a complete thermodynamic description of the $Z_{1/2}$ electron trap, and the two major boron-related hole traps, i.e. the *deep* boron, and the *shallow* boron states, with a special attention on entropy factors and capture energy barriers. DLTS analysis of n-type 4H-SiC was performed by probing the n-type side of a p^+-n asymmetrical junction, before and after proton implantation - where the implantation step is mainly used to push the concentration of $Z_{1/2}$ (E_c – 0.67 eV) above the detection limit. The presence of boron-related defects within the n-type region was detected by electrical hole injection (junction DLTS). Two distinct *shallow* boron states, named B_1 and B_2, respectively at E_v + 0.27 eV and E_v + 0.31 eV were identified by DLTS using high resolution GS4 weighting function, while a single state placed at E_v + 0.57 eV was assigned to the D-center, as reported in literature. Entropy factors and capture barriers were derived from capture rate measurements, according to the multiphonon emission model [5]. A large temperature dependence for minority carrier capture rate of *shallow* boron traps was observed for values of forward bias close to the 4H-SiC bandgap (around 3.2 eV), and the influence of forward bias - proportional to the injected holes density - on capture cross-section and capture barrier was investigated. Capture rate measurements on the D-center also highlighted the presence of two different capture mechanisms. Further targeted DLTS measurements confirmed the existence of population of deep states within the D-center peak region, which are usually not resolved by classic DLTS analysis. Two levels, named D_1 and D_2, respectively at E_v + 0.57 eV and E_v + 0.47 eV, were found. Capture and emission DLTS experiments were combined to give an overall thermodynamic description of the analysed deep states.

Experimental

Junction DLTS measurements were performed on 4H-SiC P-I-N diodes [6]. The devices were realized by CVD epitaxial growth of a 120 µm thick n-type (2e14 cm^{-3}) layer on n^+ substrate – 4° off-cut toward the [11$\bar{2}$0] direction – terminated with a 1e16 cm^{-3} n-buffer layer. The p-type side of the junction – 0.9 µm p-emitter (2e18 cm^{-3}) layer + 0.25 µm p-contact (1e19 cm^{-3}) – was realized by Mesa etching and contacted by about 2 um TiW/Al.

Proton irradiation was employed to push the concentration of $Z_{1/2}$ trap above the detection limit for DLTS analysis. Protons were implanted at 1 MeV with doses ranging from 5e7 to 5e9 cm^{-2}. DLTS measurements were carried out using the highest dose reported.

Capacitance-Voltage (CV) measurements were used to extract the net doping (N_D – N_A) concentration and depth profile. CV and DLTS measurements were performed using a HP 4280 capacitance meter, and a HP 8112a 50 MHz Pulse Generator operating at a test frequency of 1 MHz. Sample stage cooling was performed by liquid nitrogen dipping of a DLS cryostat (max temperature 380 K). Heating and temperature monitoring by LakeShore 335 Cryogenic Temperature Controller.

DLTS measurements were carried out using a reverse bias of -20 V, and pulse voltages of +20 V for $Z_{1/2}$ analysis. Minority carrier traps (boron-related defects) were detected by electrical hole injection using forward biases ranging between +3 V – meaning pulse voltages of +23 V – and +9 V. DLTS spectra were recorded in the temperature range 100-350 K, by using both Lock-in and high-resolution GS4 weighting function for fine structure identification.

The temperature dependence of deep states was investigated through capture rate measurements. In this experiment the DLTS peak signal of a given trap is recorded for several time windows, at constant temperature, as a function of the filling pulse duration. In the ideal case the curve obeys equation (1):

$$\frac{S}{S_{max}} = 1 - e^{-\tau^{-1}t}. \quad (1)$$

Where S is the DLTS signal and τ^{-1} is the capture time constant, which is equal to the sum of the emission and capture rates $e_n + c_n$ for electron traps in n-type material, and to $e_p + c_n + c_p$ for hole traps, again in a n-type material.

Since the emission rates are given by the time windows, the capture rates can be derived from time constant measurements. There are at least two methods to extrapolate the time constant from a capture curve. For example, one can take the time pulse for which $S/S_{max} = 1 - e^{-1} \approx 0.632$. Another approach is to fit the straight-line $l_n (1 - S/S_{max}) = -\tau^{-1} t$, as reported in [7]. Both methods suffer of a certain degree of uncertainty, but if the curve is ideal and the signal-to-noise ratio is high (e.g., above 100) the former is less time-consuming. We used the first method for our studies. From the capture time constant the temperature-dependent capture cross-section is derived using the equations (2, 3):

$$c_n = \sigma_n \langle v_n \rangle n_0. \quad (2)$$

$$c_p = \sigma_p \langle v_p \rangle p(V_f). \quad (3)$$

Where $\sigma_{n\,(p)}$ is the capture cross-section of electrons (holes), $\langle v_{n\,(p)} \rangle = \left(3k_B T/m^*_{n\,(p)}\right)^{1/2}$ is the average thermal velocity of electrons (holes), n_0 is the doping concentration in the n-type region, extracted from the depletion CV characteristics, and $p(V_f)$ is the forward bias-dependent injected hole density.

If capture occurs by multiphonon emission [5], the temperature dependence of σ follows the exponential law (4):

$$\sigma_{(T)} = \sigma_\infty e^{-E_\sigma/k_B T}. \quad (4)$$

By fitting Eq. 4 for different time windows, the true capture cross-section σ_∞ and the capture energy barrier E_σ for the given trap are obtained. Combining these quantities with activation energy E_a and apparent capture cross-section σ_a from the classic DLTS thermal experiment gives the entropy and enthalpy, according to equations (5, 6):

$$E_a = \Delta H + E_\sigma. \quad (5)$$

$$\frac{\sigma_a}{\sigma_\infty} = e^{\Delta S/k_B}. \quad (6)$$

The energy position of the trap, referred to as $E_c - E_t$ for electron traps, and $E_t - E_v$ for hole traps is then given by the free energy of activation $\Delta G = \Delta H - T\Delta S$.

For extrapolation of true hole capture cross-section from DLTS capture rate measurements, the forward bias dependence of injected hole density was simulated using Lumerical Inc. CHARGE solver. Input parameters for 4H-SiC were taken from NSM archive [8].

Results and Discussion

DLTS and junction DLTS spectra. Lock-in ΔC/C spectra of majority carrier traps in 4H-SiC samples are plotted in figure 1. Proton irradiation enables the detection of several deep states. The M_1 peak is a metastable state that can be suppressed using a lower reverse voltage. The S_1 and S_2 states – assigned to silicon vacancy, V_{Si} (2-/3-) and V_{Si} (-/2-) charge states [9] – are strongly reduced after annealing at 300°C. The $Z_{1/2}$ peak is assigned to the (0/2-) transition from the carbon vacancy (V_C). Further Laplace-DLTS experiments have also shown that $Z_{1/2}$ consists of two components, namely

Z_1 and Z_2, ascribed to (0/2-) transitions of V_C located at hexagonal (-h) and pseudo-cubic (-k) sites of the 4H-SiC crystal, respectively [10, 11].

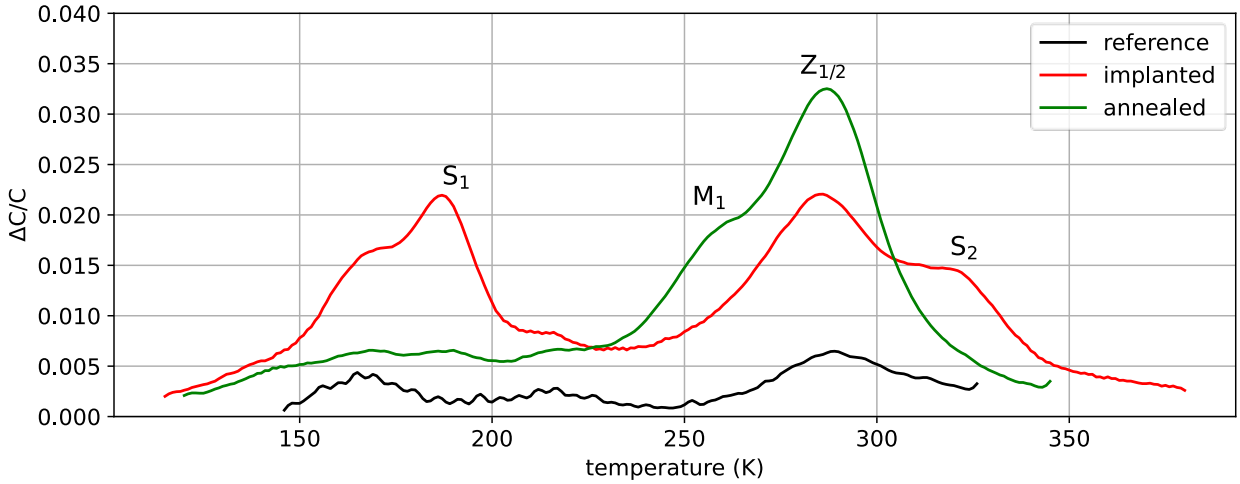

Fig. 1. Lock-in DLTS ΔC/C spectra of 4H-SiC samples, before (reference, black line) and after (implanted, red line) proton implantation (H^+ 1 MeV, 5E9 cm^{-2}) and subsequent dynamic annealing at 300°C for 1 h (annealed, green line). Reverse bias -20 V. Pulse voltages +20 V, 50 ms. Time window 0.64 s.

In figure 2, the high resolution GS4 weighting function ΔC/C spectra recorded under electrical hole injection conditions, using a forward bias of +3 V during the trap filling sequence. The minority carrier traps are identified by three prominent peaks: the *deep* boron (D-center), and the two shallow states B_1, referred as *shallow* boron, and the unidentified B_2. Recent Laplace-DLTS studies have shown that the D-center consists of two emission lines, D_1 and D_2, with activation energies for hole emissions of E_v + 0.57 eV and E_v + 0.49 eV, respectively. These emission lines have tentatively been assigned to an isolated boron sitting at the C site, -h and -k site, respectively [12].

In our experiment it was observed that proton irradiation and dynamic annealing at 300°C do not affect the D-center peak, while heavily playing on the shallow states both in terms of absolute ΔC/C value and B_1/B_2 peak ratio. The B_1/B_2 ratio after annealing is roughly the same as the reference.

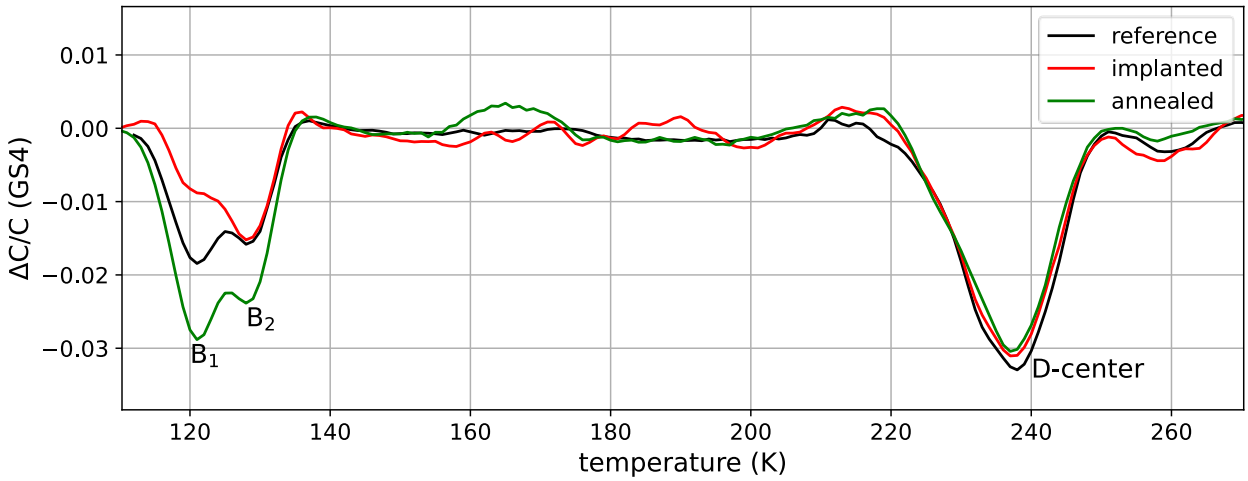

Fig. 2. GS4 DLTS ΔC/C spectra of 4H-SiC samples, before (reference, black line) and after (implanted, red line) proton implantation (H^+ 1 MeV, 5E9 cm^{-2}) and subsequent dynamic annealing at 300°C for 1 h (annealed, green line). Reverse bias -20 V. Pulse voltages +23 V, 50 ms. Time window 0.64 s.

Activation energies E_a and apparent capture cross-sections σ_a for $Z_{1/2}$, B_1, B_2, and D-center states, extracted from the Arrhenius plot, are reported in table 1. According to Eq. 5, the activation energy E_a is here taken as the sum $\Delta H + E_\sigma$ of a general temperature-dependent capture process, where E_σ is the energy barrier for capture that can be derived from capture rate measurements, assuming a multiphonon emission mechanism, together with the true capture cross-section σ_∞.

Table 1. Trap signature resulting from Arrhenius plot. The $Z_{1/2}$ characteristics were derived using Lock-in weighting function DLTS spectra. For D-center, B_1 and B_2 trap states, high resolution GS4 weighting function was used.

	$Z_{1/2}$	D-center	B_1	B_2
E_a [eV]	0.67	0.57	0.27	0.31
σ_a [cm^2]	8.95e-15	3.03e-14	2.23e-14	1.16e-13

Capture rate measurements. Capture rates for majority and minority carrier traps can be extracted by plotting the DLTS signal of a given peak against the filling pulse duration. This experiment gives information about potential temperature dependence of the capture cross-section of the deep state, which is not explicitly given by the classic DLTS thermal emission experiment, and the capture energy barrier. Combining this information with the trap signature resulting from the Arrhenius plot (table 1) enables the determination of the free energy $\Delta G = \Delta H - T\Delta S$ of electronic activation of the deep state.

Interpretation of the capture rate experiment is quite straightforward for majority carrier traps where the charge carrier concentration is known as it corresponds to the net doping concentration, which is readily given by the depletion Capacitance-Voltage characteristics. The limit of junction DLTS in evaluating minority carrier trap properties lies in the determination of the injected minority carrier density, which is dependent on the forward bias and not always easy to measure.

Figure 3 shows a typical capture rate experiment performed on the $Z_{1/2}$ trap state. In figure 3a the relative DLTS signal S/S_{max} is plotted against the filling pulse duration. The true capture cross-section σ_∞ and the capture activation barrier E_σ are derived from the Arrhenius plot (figure 3b) built on the temperature-dependent capture cross-section (see Eq. 4).

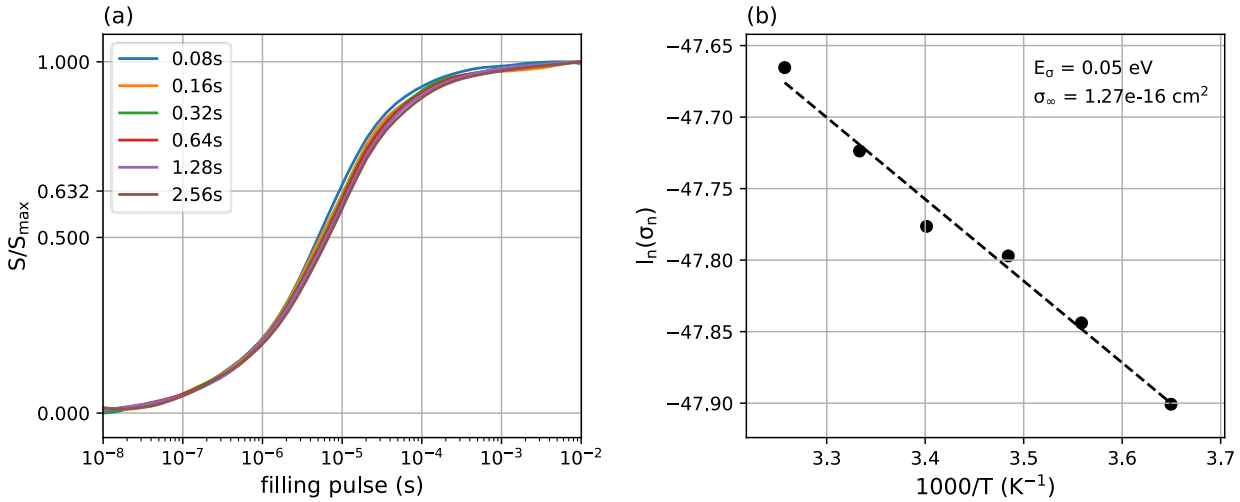

Fig. 3. (a) Relative DLTS signal S/Smax against filling pulse duration for the $Z_{1/2}$ trap state; (b) Arrhenius plot of electron capture cross-section σ_n against 1/T. Capture barrier E_σ and true capture cross-section σ_∞ are respectively derived from the linear fit slope and intercept.

In figure 4a, the capture experiment for the B_1 (*shallow* boron) trap state is shown for different values of applied forward bias pulse. The dependence of the linear fit parameters on the forward bias is made explicit in figure 4b. The true capture cross-section σ_∞ and the capture activation barrier E_σ are derived from the Arrhenius plot, according to Eqs. 3, 4. To highlight the similarity of σ_∞ and E_σ dependence on forward bias, σ_∞ is reported as $-k_B T \ln(\sigma_\infty) + A$ (where T = 120 K, A = 0.54 eV).

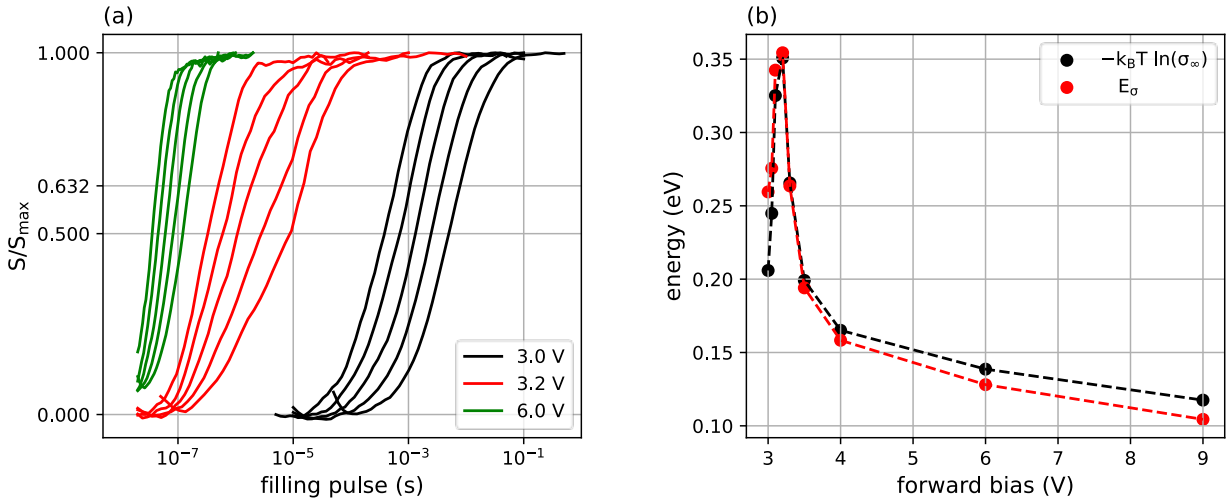

Fig. 4. (a) Relative DLTS signal S/Smax against filling pulse duration for the B_1 trap state; (b) dependence of multiphonon emission model fit on applied forward bias. Maximum values of σ_∞ and E_σ are 1e-4 cm^2 and 0.35 eV. Measurement of filling pulse is limited by the pulse generator max frequency of 50 MHz (min pulse 2e-8 s).

The same experiment performed on the D-center peak revealed the presence of two different capture mechanisms. The curves plotted in figure 5a were recorded using a forward bias of +3 V. The major capture process (D_1, left side) shows small temperature dependence, while a large dependence is visible for the second capture step (D_2, right side). In figure 5b the Arrhenius plot for the two capture processes, named D_1 and D_2, is displayed with the relative fitted capture parameters. Figure 5c shows the differential DLTS spectra recorded by varying the filling pulse duration. A time pulse of 200 ns was used to isolate the D_1 signal contribution. The difference between the long (50 ms) pulse and the short pulse corresponds to D_2 signal plus the lowering (fig. 5a) in the 10^{-6}-10^{-5} s pulse range. The Arrhenius plot of the separated signals is shown in figure 5d. It can be observed that activation energies for D levels roughly corresponds to those obtained by Laplace-DLTS measurements.

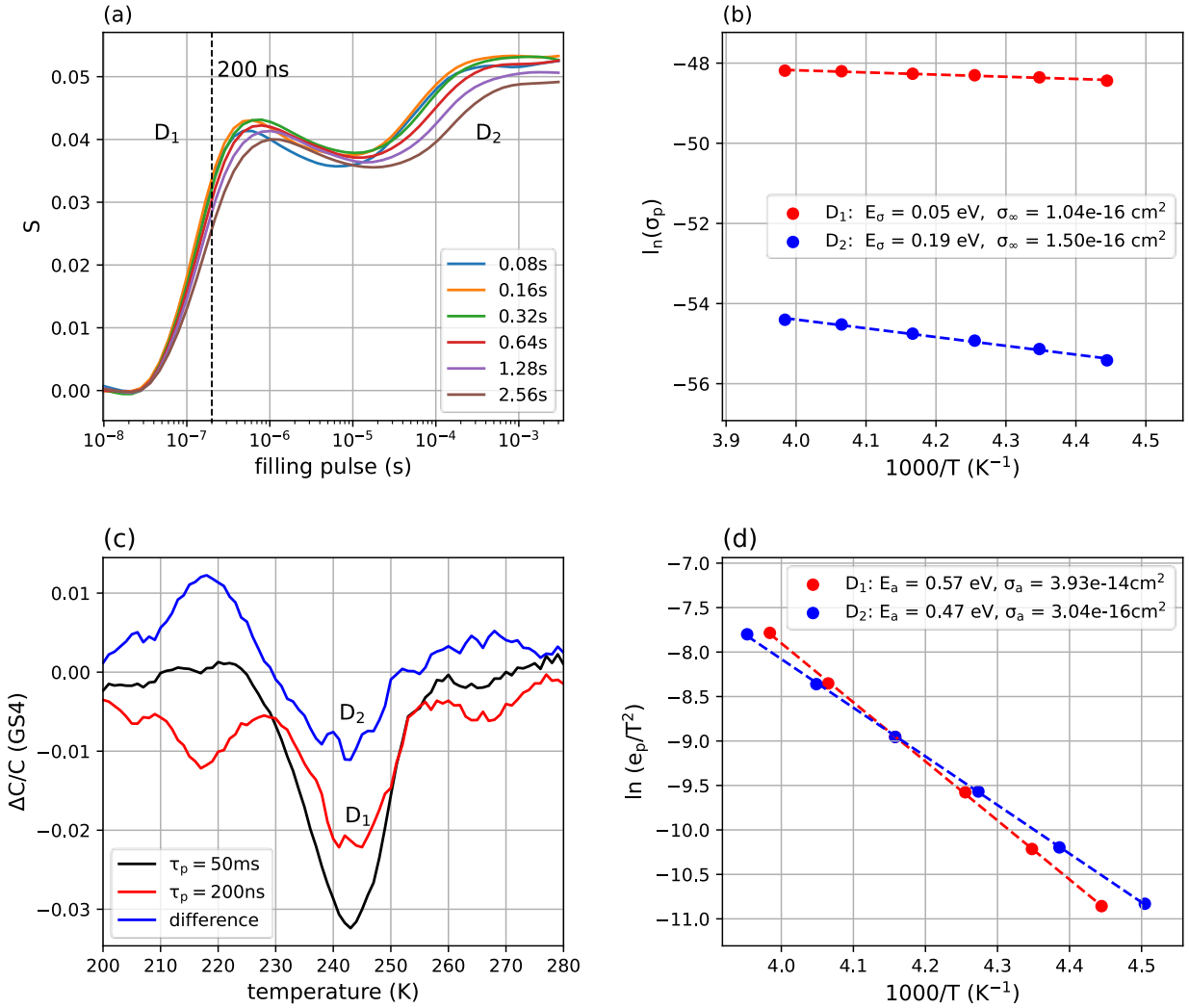

Fig. 5. (a) DLTS signal S against filling pulse duration for the D-center peak. The curve is arbitrarily separated into two regions, corresponding to different capture processes; (b) Arrhenius plot of hole capture cross-section σ_p against 1/T; (c) differential junction DLTS spectra recorded with different time pulses. The positive peak (difference, blue curve) just below 220 K was assumed to be responsible for the signal lowering in the 10^{-6}-10^{-5} s pulse range (fig. 5a); (d) Trap signatures derived from the Arrhenius plot of D_1 and D_2 peaks.

In table 2, the results of our measurements are summarized to give a full thermodynamic description of $Z_{1/2}$, B, and D levels. Due to the limits of junction DLTS experiments, only the numbers reported for $Z_{1/2}$ trap can be read as incontrovertible. Specifically, as far as the junction DLTS results interpretation is concerned, several sources of error must be considered. First, the injected minority carrier density was here estimated after electrical simulations. These data are an important part of the junction DLTS experiment and can be experimentally determined using the J-V characteristics of the injection current of the device [13]. Moreover, the capture parameters E_σ and σ_∞ reported for the B_1 level were taken from the +9 V forward bias measurement (see fig. 4b), as the lowest values obtained, but the exponential decay of the curves suggests a further lowering of these quantities. Also, while the approximation of $\tau^{-1} = c_n$ works for the $Z_{1/2}$ majority carrier trap (see Eq. 2, and text above), it is not ensured for B_1 where we considered $\tau^{-1} = c_p$, because the information about capture c_n of electrons in the minority carrier trap is missing (see Eq. 3, and text above). A rigorous procedure would imply measurements of the time constant as a function of injected hole density, in low injection regime, and extrapolation of c_n and c_p as reported by Blood and Orton [14]. In addition, as highlighted in table 2 (see notes), the forward bias dependence was not investigated for the B_2 trap, and the numbers

reported for D levels are taken at +3 V, thus not considering the actual dependence of capture parameters on the forward bias.

Table 2. Collection of thermal properties of analysed trap states. The quantities E_a, σ_a, E_σ, and σ_∞ are experimentally determined; ΔS, ΔH, and ΔG are derived from them. The experimental error on energies is around 0.01 eV.

	E_a [eV]	σ_a [cm^2]	E_σ [eV]	σ_∞ [cm^2]	$\Delta S/k_B$	ΔH [eV]	$\Delta G_{(300\ K)}$ [eV]
$Z_{1/2}$	0.67	8.95e-15	0.05	1.27e-16	4.26	0.62	0.51
B_1	0.27	2.23e-14	0.10	1.87e-14	0.17	0.17	0.16
B_2	0.31	1.16e-13	[a]0.10	[a]1.87e-14	1.82	0.21	0.16
D_1	0.57	3.93e-14	[b]0.05	[b]1.04e-16	5.94	0.52	0.37
D_2	0.47	3.04e-16	[b]0.19	[b]1.50e-16	0.71	0.28	0.26

[a] Bias-dependent capture measurements were not performed for the B_2 trap; E_σ and σ_∞ values are assumed to be roughly the same as for B_1.

[b] The forward bias dependence was not investigated for the D levels; E_σ and σ_∞ values were measured at +3 V and must be read with care.

Nonetheless, the estimated capture cross sections, capture barriers and entropy factors are valuable numbers, since they can be used to estimate the overall lifetime of the charge carriers, and to obtain a firm identification of the defect origin, in combination with theoretical modelling.

By the way, some interesting considerations can be drawn from our experiments. For example, the two contributions to the D-center observed here show substantially different characteristics, even though they overlap in the DLTS spectrum. D_1 exhibits a substantial entropy factor, while D_2 displays a large capture barrier. These results suggest that capture by D_1 is associated with a significant change in lattice vibrational entropy and thus a change in the bonding configuration, while the capture barrier measured for D_2 indicates a large temperature dependence for hole capture by the deep state, but with a small ΔS. A difference in ΔS can also be observed for the two *shallow* B defects, while both exhibit a large apparent capture cross section and a small capture barrier. As in general expected for shallower states, the entropy factors are relatively small for B trap states, thus indicating small changes in the bonding configuration associated with the hole capture process. Further forward bias-dependent capture measurements on B_2 and the D levels could confirm or disprove these data.

Reasonably, these properties could be used to further extend our understanding of the main lifetime-limiting defects in 4H-SiC and support theoretical modelling to establish their microscopic origin.

Conclusions

Emission and capture junction DLTS measurements were performed to obtain information about majority and minority carrier prominent traps in n-type 4H-SiC. Proton irradiation was employed to detect majority carrier deep states. High resolution GS4 weighting function DLTS spectra enabled characterization of an unidentified trap level, here named B_2, within the *shallow* boron (B_1) peak region.

True capture cross-sections and capture energy barriers were extrapolated from capture rate DLTS measurements. Investigation of the forward bias dependence of B_1 trap state revealed an unexplained large temperature dependence of capture parameters for values of forward bias close to the material bandgap (around 3.2 eV), with estimated maximum values of true capture cross-section and capture energy barrier of 1e-4 cm^2 and 0.35 eV (Fig. 4). Capture rate measurements on D-center DLTS peak revealed the presence of two different capture processes, named D_1 and D_2, plus a possible emission process in the 10^{-6}-10^{-5} s pulse range (Fig. 5a). Based on capture measurements, the separation and characterization of D_1 and D_2 levels was obtained from the difference of long and short filling pulses DLTS spectra (Figs. 5c, 5d).

Capture and emission experiments were combined to give the thermal properties reported in table 2. As evidenced, even though junction DLTS represents an alternative method to obtain information on minority carrier traps, thermodynamic data derived from capture experiments should be read with care, and compared to the more reliable majority carrier DLTS measurements to have an idea of what are the limits of the technique and, where possible, to find correction factors which can serve to calibrate a valid experimental protocol useful for further measurements.

CRediT author contribution statement

Orazio Samperi: Investigation, Visualization, Validation, Writing – Original Draft, Writing – Review & Editing. **Lasse Vines:** Conceptualization, Resources, Investigation, Supervision, Writing – Review & Editing. **Anders Hallén:** Conceptualization, Resources, Supervision, Writing – Review & Editing. **Maria Elena Fragalà:** Supervision, Writing – Review & Editing.

Declaration of competing interests

The authors declare that they have no known competing financial interests or personal relationships that could have appeared to influence the work reported in this paper.

Acknowledgments

The Research Council of Norway is acknowledged for the support to the Norwegian Micro- and Nano-Fabrication Facility, NorFab, project number 295864.

Data availability

The data that support the findings of this study are available from the corresponding author upon reasonable request.

References

[1] N.T. Son, X.T. Trinh, L.S. Løvlie, B.G. Svensson, K. Kawahara, J. Suda, T. Kimoto, T. Umeda, J. Isoya, T. Makino, T. Ohshima, and E. Janzén, "Negative-U system of carbon vacancy in 4H–SiC," Phys. Rev. Lett. 109, 187603 (2012).

[2] P.B. Klein, B.V. Shanabrook, S.W. Huh, A.Y. Polyakov, M. Skowronski, J.J. Sumakeris, M.J. O'Loughlin; Lifetime-limiting defects in n^- 4H-SiC epilayers. Appl. Phys. Lett. 30 January 2006; 88 (5): 052110.

[3] L. Storasta, P. Bergman, E. Janzén, and C. Hallin, Mater. Sci. Forum 389-393, 549 (2002).

[4] Misagh Ghezellou, Piyush Kumar, Marianne E. Bathen, Robert Karsthof, Einar Ö. Sveinbjörnsson, Ulrike Grossner, J. Peder Bergman, Lasse Vines, Jawad Ul-Hassan; The role of boron related defects in limiting charge carrier lifetime in 4H–SiC epitaxial layers. APL Mater. 1 March 2023; 11 (3): 031107.

[5] Blood P and J. W Orton, The Electrical Characterization of Semiconductors: Majority Carriers and Electron States, Academic Press 1992, p. 433.

[6] K. Tian, J. Via, K. Elgammal, A. Schöner, W. Kaplan, R. Karhu, J. Ul-Hassan, A. Hallén. Modelling the static on-state current voltage characteristics for a 10 kV 4H-SiC PiN diode. Material Science in Semiconductor Processing 115, 105097 (2020).

[7] E Omotoso et al 2020 Mater. Res. Express 7 025901.

[8] https://www.ioffe.ru/SVA/NSM/Semicond/SiC/bandstr.html.

[9] Bathen, M.E.; Galeckas, A.; Müting, J.; Ayedh, H.M.; Grossner, U.; Coutinho, J.; Frodason, Y.K.; Vines, L. Electrical charge state identification and control for the silicon vacancy in 4H-SiC. NPJ Quantum Inf. 2019, 5, 111.

[10] Capan, I.; Brodar, T.; Pastuović, Z.; Siegele, R.; Ohshima, T.; Sato, S.I.; Makino, T.; Snoj, L.; Radulović, V.; Coutinho, J.; et al. Double negatively charged carbon vacancy at the h- and k-sites in 4H-SiC: Combined Laplace-DLTS and DFT study. J. Appl. Phys. 2018, 123, 161597.

[11] Capan, I.; Brodar, T.; Coutinho, J.; Ohshima, T.; Markevich, V.P.; Peaker, A.R. Acceptor levels of the carbon vacancy in 4 H-SiC: Combining Laplace deep level transient spectroscopy with density functional modeling. J. Appl. Phys. 2018, 124, 245701.

[12] Capan, I.; Brodar, T.; Yamazaki, Y.; Oki, Y.; Ohshima, T.; Chiba, Y.; Hijikata, Y.; Snoj, L.; Radulović, V. Influence of neutron radiation on majority and minority carrier traps in n-type 4H-SiC. Nucl. Inst. Methods Phys. Res. 2020, B478, 224–228.

[13] Blood P and J. W Orton, The Electrical Characterization of Semiconductors: Majority Carriers and Electron States, Academic Press 1992, p. 567.

[14] Blood P and J. W Orton, The Electrical Characterization of Semiconductors: Majority Carriers and Electron States, Academic Press 1992, p. 639.